# Melanoma detection on dermoscopic images using  superpixels segmentation and shape-based features

Diego Patiño, Alberto Ceballos-Arroyo, Jairo Rodriguez-Rodriguez, German Sanchez-Torres, John Branch-Bedoya

**SPIE.**

# Melanoma Detection on Dermoscopic Images using Superpixels Segmentation and Shape-Based Features

Diego Patiño [a] [ID] , Alberto M. Ceballos-Arroyo[a] [ID] , Jairo A. Rodriguez-Rodriguez[a] [ID] ,
German Sanchez-Torres[b] [ID] , John W. Branch-Bedoya[a] [ID]

[a]Department of Computer and Decision Sciences, Universidad Nacional de Colombia - Sede Medellín, Av. 80 #65 - 223, Medellín, Colombia;
[b]Faculty of Engineering, Universidad de Magdalena, Cl. 32 #22 - 08, Santa Marta, Colombia

## ABSTRACT

In this work, we present a shape-based approach to automatic skin lesion segmentation and classification in dermoscopic images. We aim to differentiate three types of lesion 1) common nevi, 2) atypical nevi, and 3) melanomas by exploring the morphology features of segmented skin lesions. Our method is an attempt to design a computer-aided ABCDEs of melanoma, where the **A**symmetry and **B**order components are estimated using morphological features. The lesions are first segmented using a super-pixel merging strategy with an RGB criterion. Later, the segmentation method was evaluated on the PH$^2$ dataset, and compared with other state-of-the-art skin segmentation methods. The classification was also conducted on the PH$^2$ dataset through a 10-fold cross-validation set-up with a training and testing set partition of 90% and 10% respectively. We employed logistic regression, SVM and a neural network as classification algorithms. The best performances was 86.5% on average with the neural network.

## 1. INTRODUCTION

Melanoma is the deadliest form of skin cancer, and it can occur in any type of skin. Due to its mortality rates, the early detection of malignant melanoma in dermoscopic images is crucial and since it is vital to detect it in the early stages of the disease in order to provide proper treatment for the patient. For this reason, physicians have developed two specific informal strategies for the early recognition of the disease such as the ABCDE of melanoma[1] and the Ugly Duckling sign.[2]

The "ABCDE" rule was designed for human-based visual analysis of a skin lesion. It uses different visual cues to classify the lesion type: (A) Asymmetry, (B) irregularity of the Borders, (C) presence of specific Colors, (D) lesion shape and size, and (E) evaluation of the lesion evolution over time. Some of these cues can be translated into a computer-aided strategy to create an automatic framework for skin lesion classification which can become very helpful in facilitating the early detection of cancers for dermatologists.

This paper focuses on constructing a fully-automatic method to identify and classify skin lesions in dermoscopic images. We used the superpixel merging approach defined in the work Patiño *et al.*[3] to extract a segmentation mask. Later, a set of shape-based features extracted from this mask are computed. The main idea is that shape-based features can capture the A and B components of the ABCDE rule. Later, these components were used as input features for classification experiment to discriminate between healthy skin lesions and melanomas.

The (A) and (B) visual cues depended strongly on the morphological properties of the border of a skin lesion. These cues relate to smoothness and invariance to reflections around a given axis passing through the centroid of the object. Hence, a shape feature can be created measuring how similar the border of a lesion is w.r.t its reflected version around a certain axis. The major and minor axes of the minimum enclosing ellipse are used here because they already define the two main directions of symmetry. Moreover, the smoothness of the border can also be used to extract additional shape features because melanoma skin lesions tend to have irregular edges.

Additionally, (C) can be seen as local color patterns arising over the surface of the lesion. Hence, we compute first-order textures over the mean color of each superpixel instead of using each pixel in the lesion region. By doing this, we take advantage of the superpixel segmentation to create yet another visual inspired feature.

We tested our methodology on the PH$^2$.[4] This dataset consists of 200 images divided into three groups: common lesions, atypical nevi, and melanomas. We compared our results with previous work in state-of-the-art.

The rest of this document is organized as follows: Section 2 reviews previous work on skin lesion segmentation and classification. Section 3 presents an overview of the employed segmentation method. In section 4, we introduce a new set of features, engineered to exploit the morphological and color properties of the segmented lesion. In Section 5, experimental results over the PH$^2$ are presented. Finally, Section 6 concludes the paper and states potential future work.

## 2. RELATED WORK

**Skin Lesion Segmentation**   Many segmentation algorithms have been proposed in the literature to deal with the problem of accurately segmenting skin lesion on dermoscopic images while classifying several types of lesions.[5–8] Such approaches share a common structure that consists of first removing artifacts such as hair and oil bubbles in the images, followed by the segmentation of the skin lesion using different combinations of thresholding, clustering, and morphological operations.

One of the more representatives proposals on the subject is that of Pennisi *et al.*,[9] where the authors defined a complete framework for skin lesion segmentation and classification based on Delaunay Triangulation. The polygons in such triangulation adapt to the lesion border according to a color criterion. In an earlier work, Sabbaghi *et al.*[10] also presented an interesting approach for this type of classification. They used the QuadTree algorithm to subsequently group pixels with similar color properties and then analyzed which colors are present in each type of lesion. The authors did not perform any segmentation, and instead they carried out the classification using the whole set of pixels in the images.

**Skin Lesion Classification**   Several proposals in the literature have approached the problem of skin lesion classification.[11–13] Catarina Barata *et al.*[11]  presented two strategies for detecting melanoma in dermoscopy images: global and local methods. To classify skin lesions they used the former, while the latter strategy was used to extract a bag-of-features set of descriptors. Color and texture features were also used, achieving a sensitivity of about 96% and a specificity of approximately 80%. No information about the shape of the lesion was included in the study. In another work, Khaled Abu *et al.*[12] discussed the classification system for skin cancer to detect whether a melanoma is benign or malignant. In this, other lesion types are not included. i.e., they did not seem concerned about Nonmelanocytic skin lesion. On the other hand, Ballerini *et al.*[13] presented a method to distinguish among five skin cancers using color and texture, but melanomas are not included.

The number and type of features over different approaches in the literature vary significantly. In general, authors used the set of features that they believe is more convenient for the classification task.

**Shape Features**   Shape features has been widely used in literature to describe the morphological properties of an object.[14] They are all based on geometric information of the object such as contours, geometric moments, medial axis,[15] or spectral signatures.[16] Shapes of objects arise naturally in many fields where the geometric information of volumes or surfaces plays an essential role in the subject of study. A straightforward example is perhaps medicine, where many clinical applications such as radiotherapy planning, MRI analysis, image-guided surgery, or treatment evolution heavily rely on the analysis and processing of both 2D and 3D data. Nonetheless, there are many other domains where understanding shapes prove to be a useful tool. Such domains include non-destructive object study and reconstruction in archaeology and cultural heritage; object classification and retrieval from large collection of images; human action and pose recognition for gaming and entertainment; environment sensing in robot navigation and planning; or industry for automatic visual quality inspection of product defects.[17]

In this paper, we aim to automatically identify types of skin lesion hoping to be able to differentiate between healthy skin lesion and melanomas: Melanocytic skin lesions (MSLs) and Non-melanocytic skin lesions (NoMSLs). Our approach leverage shape-based features to perform the classification. These feature are computed using the morphology of the segmented lesion.

# 3. SEGMENTATION

In this section, we describe our method for skin lesion segmentation in dermoscopic images. First, we use SLIC algorithm to obtain an over-segmentation of the original dermoscopic image $I$. Later, we greedily merge all the superpixels into two regions: lesion and healthy skin. The morphology of the lesion is captured via shape-based features on the segmented image. These features are employed as input data for a set of classifiers.

## 3.1 Superpixel segmentation

Superpixels methods over-segment an image by grouping pixels into units called superpixels. One of the most well-known algorithms for superpixel segmentations is Simple Linear Iterative Clustering (SLIC) developed by Achanta *et al.* in 2012.[18] In SLIC, pixels are grouped using k-means algorithm with color intensities plus $(i, j)$ coordinates as the features of each pixel. SLIC is, in essence, a modification of basic k-means algorithm that applies constraints to prevent that unconnected pixels could belong to the same superpixel.

For segmenting the skin lesion from the whole image, our method performs a SLIC superpixel segmentation on the RGB dermoscopic images. Ideally, in the over-segmented image, the superpixel's boundary should match partially the boundary of the object that is intended to segment.

SLIC requires the parameter $k$ that indicates the desired number of superpixels in the resulting image. We experimented with different values of the parameter, and set its value empirically to $k = 400$. With higher values of $k$, too much over-segmentation is done, resulting in longer execution times with no significant improvement in the resulting segmentation. On the other hand, low values of $k$ fail at fitting the border of the lesion in the image. Figure 1 shows the resulting super-pixel segmentation for two images and four different values of parameter $k$.
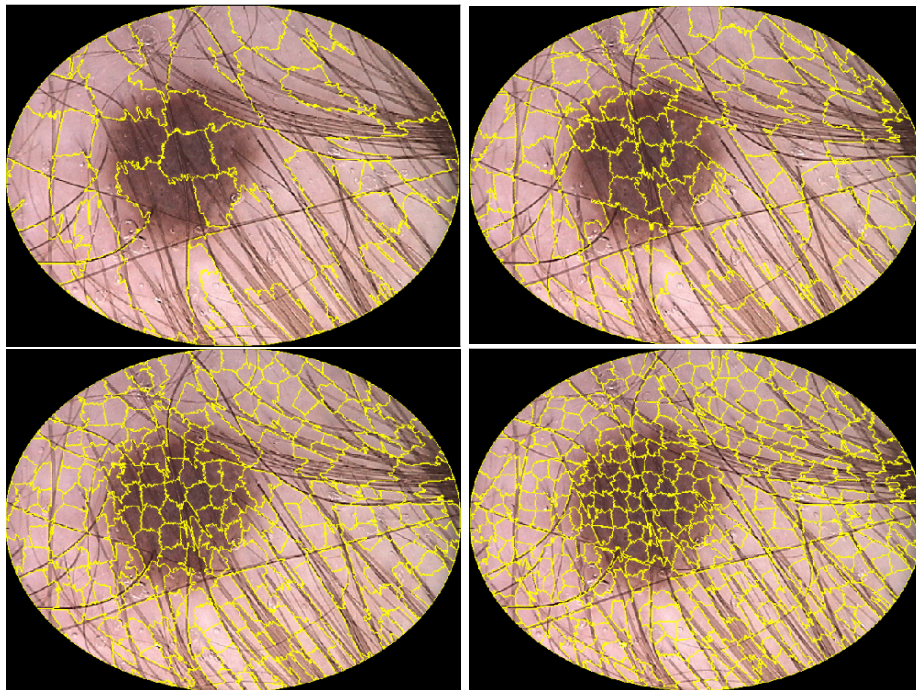


Figure 1: SLIC segmentation for several $k$ values. Left to right and top to bottom: $k = 100, 200, 400, 600$. It can be observe that lower values under-segment the lesion, while larger values are computationally more expensive without improving the results significantly

All original images have a dark shadow around the four corners of the image. This is an effect of the illumination setup in the dermatoscopy device that was used to capture the images. A binary mask is applied to the resulting SLIC segmentation to remove such effect. The mask is defined as the maximum ellipse inscribed in the image area.

## 3.2 Superpixel merging

SLIC segmentation produces an over-segmented image with approximately $k$ pieces. Hence, a merging operation must be done to separate the skin lesion (foreground superpixels) from the region containing pixels with no lesion (background superpixels). From this representation, a Region Adjacency Graph (RAG) is constructed over the superpixels, and their mean color is computed.

Superpixel merging is then done by greedily combining pairs of nodes using the euclidean distance of the mean color as a criterion. The merging is applied to each node until only two regions remain: foreground and background. If the color distance between two nodes is less than a threshold $t$, the two nodes will merge and a new node is created. Next, the new node's properties are calculated based on those of the nodes that were merged. A binary search determines the optimal threshold by running the merging procedure with several values of $t$.

## 3.3 Post-processing

The merging produces a label image $L$ where each superpixel is associated to an integer value. At this stage of the segmentation process it is not possible to determine whether a label corresponds to background or to skin lesion. Therefore, we create image $O$ by applying adaptive equalization to a gray-scale version of the original image, and subsequently segmenting it using Otsu's thresholding. Each label in $L$ is compared with $O$ by computing the Jaccard similarity index between the two areas. The label with the maximum Jaccard index is selected as the final segmented image after applying binary fill holes and a morphological dilation with a disk-shaped structural element of radius $r = 8$. Figure 2 show the results of the segmentation pipeline. The binary fill holes operation has the effect of creating a unique closed curve around the lesion.
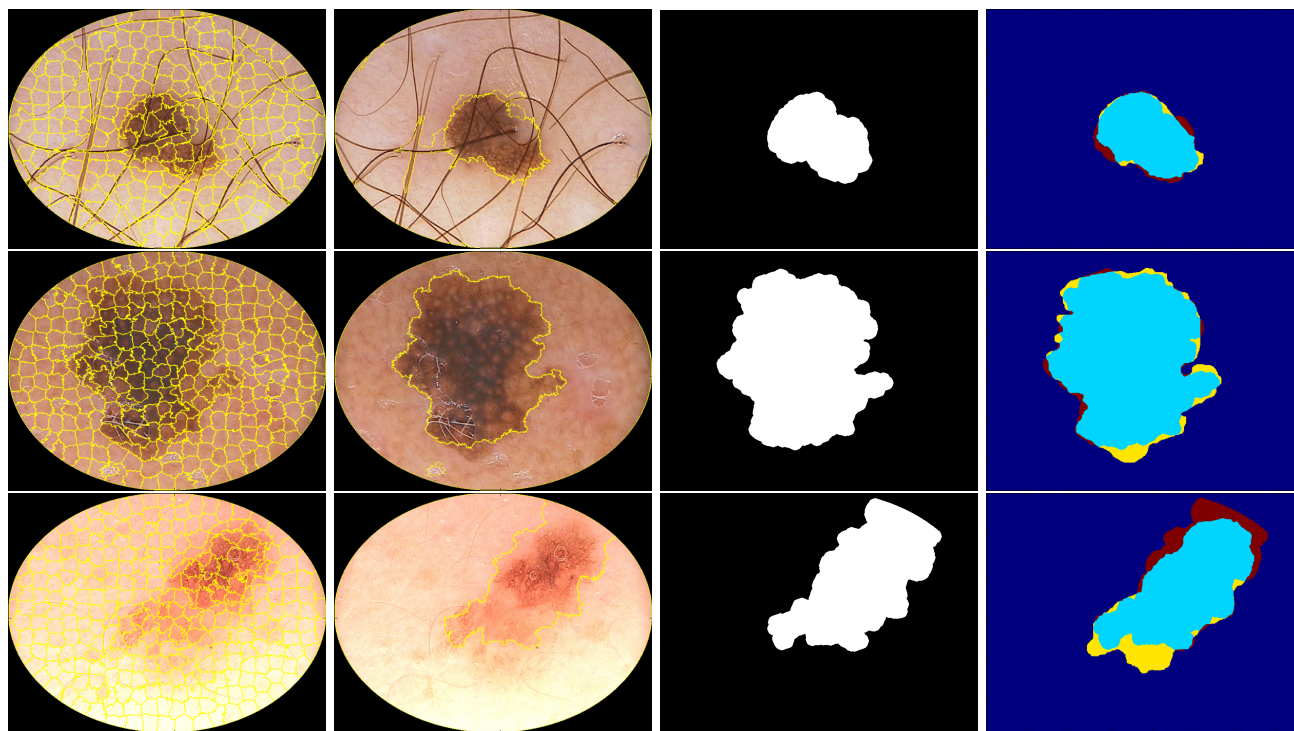


Figure 2: Segmentation results for three different images. From left to right: Original image with SLIC segmentation ($k = 400$), merged superpixels, final segmentation binary mask, and ground-truth comparison. True positives: light blue, true negatives: dark blue, false negatives: yellow, and false positives: dark red.

# 4. CLASSIFICATION

The classification was done by extracting shape-related features from the segmented lesion regions using the methodology from Section 3. We aimed to design features inspired by the visual cues of the ABCDE criterion for

melanoma detection. Mainly, we associated shape-related features with (A)symmetry, and (B)order. Moreover, we also included (C)olor features as first-order textures over the superpixel mean colors.

## 4.1 Data set

To test the proposed approach, we used the PH$^2$ dataset[4] released by the Universidade do Porto in collaboration with the Hospital Pedro Hispano in Matosinhos, Portugal. This dataset contains 200 RGB images of dermoscopic lesions. It includes 80 common nevi, 80 atypical nevi, and 40 melanomas. For each image, there is a manually generated ground-truth segmentation of the skin lesion.

## 4.2 Asymmetry features

Symmetry can be defined as the property of an abstract object to preserve its geometric properties when some isometric transformations (translation, rotation, and reflections) are applied. We developed new features to classify skin lesions by measuring how much the symmetry is not invariant to the above mentioned transformations. Skin lesions can appear in different positions and rotations without affecting their nature. Hence, we chose reflections as the isometric transformation on which to base our asymmetry feature.

Let $\Omega$ be the 2D region surrounding a skin lesion. Our asymmetry feature is estimated by reflecting the contour of the lesion ($\delta\Omega$) around the major and minor axes of the minimum ellipse enclosing $\Omega$. These two axes already offer a measure of symmetry; however, assuming the object is a perfect ellipse does not take into account variations on both sides of the contour that break the reflection symmetry.

A reflection of a 2D object around an axis $v$ can be parametrized by a transformation matrix

$$R = I - 2d^\top d, \tag{1}$$

where $I$ is the identity matrix in 2D, and $d$ is a unit row vector orthogonal to $v$. Let us denote $X \in \mathbb{R}^{2 \times m}$ the matrix containing all the points in $\delta\Omega$ as columns; the matrix $\hat{X} = RX$ contains all the points of the contour $\delta\Omega$ reflected around the plane defined by $v$. In this works, $v$ can be either the major or minor axis.

Next, we compute the asymmetry features taking both the Hausdorff Distance and the Jain-Dubuisson dissimilarity[19] between $X$ and $\hat{X}$ for the major and minor axis reflections:

$$F_{\text{asymmetry}} = [F_{\text{hauss-minor-axis}}, F_{\text{hauss-major-axis}}, F_{\text{jain-minor-axis}}, F_{\text{jain-major-axis}}] \tag{2}$$

The discriminative potential of $F_{\text{asymmetry}}$ arises from the fact that when a lesion $\Omega$ is perfectly symmetric, the Hausdorff distance as well as the Jain-Dubuisson dissimilarity will be 0. If any segment of the contour breaks the symmetry, both metrics will have a greater positive value proportional to the level of asymmetry. In this way, we encode the idea behind the A and B visual cues of the ABCDE of melanoma.

## 4.3 Border features

For the border features, we considered a smoothness criterion due to the fact that nevi and atypical nevi tend to have smooth contours. On the other hand, in melanomas the contour is highly irregular. To compute the border features we first expressed $\delta\Omega$ as the periodic function

$$\gamma(t) = \sqrt{(x(t) - x_0)^2 + (y(t) - y_0)^2}. \tag{3}$$

Here, $(x_0, y_0)$ is the centroid of the lesion, $t \in [0, n]$, and $n$ is the number of points in $\delta\Omega$. Using the Discrete Fourier Transform (DFT) and its inverse, we define $\hat{\gamma_m}(t)$ as the reconstructed version of $\gamma$ using only the first $m$ coefficients of the DFT. The intuition here is that the smoother $\gamma$ is, the fewer coefficients will be needed to achieve a good reconstruction. Thus, the border features are defined as:

$$F_{\text{border}} = [\ MSE(\gamma, \hat{\gamma_1}) \quad MSE(\gamma, \hat{\gamma_2}) \quad ... \quad MSE(\gamma, \hat{\gamma_m})\ ] \tag{4}$$

The MSE is the Mean Square Error computed over all the points in the contour.

If we assume that for a smooth contour only the first $k_1$ elements of $F_{\text{border}}^{(1)}$ are significantly greater than zero, then in a less smooth contour $F_{\text{border}}^{(2)}$, the number of elements that are significantly greater than zero will be $k_2$ with $k_1 < k2$. Consequently, the direction in the $m$-dimensional euclidean space between $F_{\text{border}}^{(1)}$ and $F_{\text{border}}^{(1)}$, expressed as $\angle(F_{\text{border}}^{(1)}, F_{\text{border}}^{(2)})$ will be different than "0". Figure 3 shows how the contour highlights the asymmetry and border features.
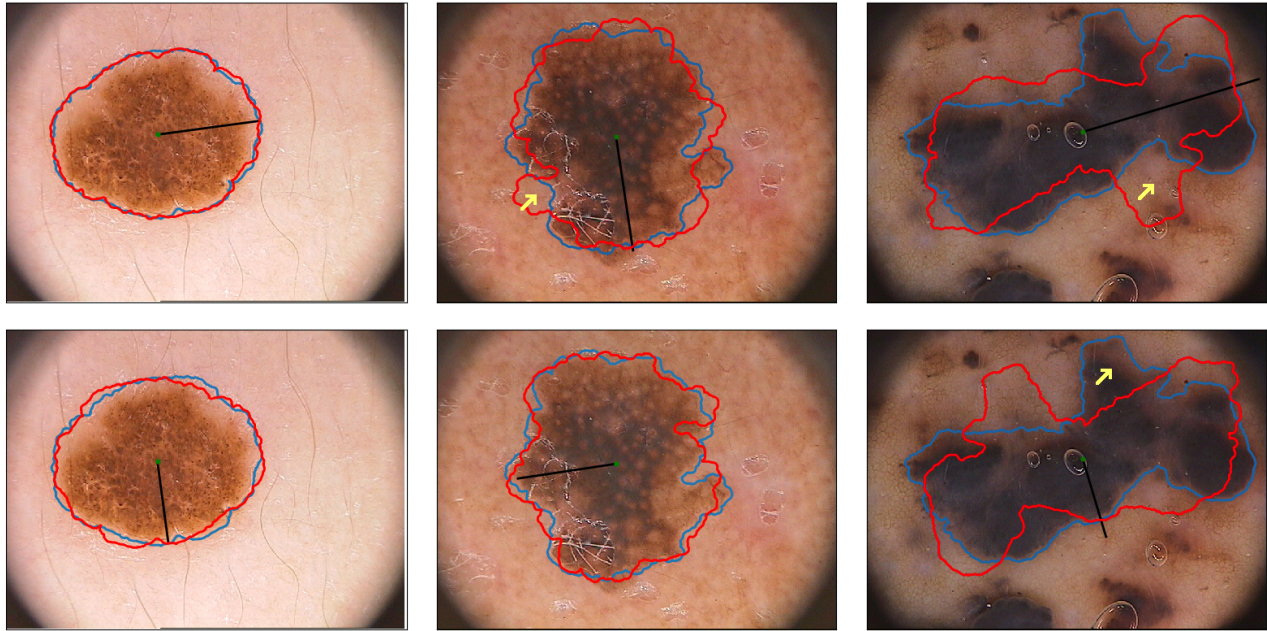


Figure 3: Graphical representation of symmetry and border smoothness for three different lesions: common nevi (col. 1), melanoma (col. 2), melanoma (col. 3). The blue curve is the border of the lesion $\Omega$, and the red curve is its reflected version w.r.t the major axis (first row) and the minor axis (second row). It can be seen how the border is smoother in healthy skin, and how the differences between the contour and its reflection highlights asymmetries of the lesion. The yellow arrows point to such differences to facilitate the interpretation.

## 4.4 Color features

In order to capture color information, we also computed a set of first-order textures $F_{\text{color}}$. However, they were applied to the superpixel segmentation, instead of directly to the individual pixels in the lesion. Each superpixel represents an area of uniform color inside the lesion. Therefore, by computing the color textures over them, we are obtaining an indication of color distribution over a sort of semantic partitioning of the lesion. We used the mean, standard deviation, skewness, entropy, and kurtosis from the "a" and "b" channels of the Lab color-space to avoid the effect of illumination changes. The color assigned to every superpixel is the mean color over all the pixels that belong to it.

## 5. EXPERIMENTAL RESULTS

To compare our segmentation approach with other methods, we performed the same set of tests presented in the work of Pennisi et al.[9] and Patiño et al.[3] Hence, we used PH[2] ground-truth lesion segmentation to evaluate the outcome of our algorithm using four metrics: sensitivity, specificity, accuracy, and F-measure. Table 1 shows the segmentation results as presented by Pennisi et al.,[9] but extended with our results.

The presented strategy achieved significantly better sensitivity than the previous work. This means that pixels belonging to a skin lesion are segmented correctly in a higher proportion compared with other methods

(fewer false positives). A similar situation occurs with the F-measure. In this case, better accuracy was also obtained in all test cases, with the exception of melanoma. However, as opposed to the other three metrics, specificity was lower when compared to the methods in the literature. This means our method tends to classify healthy pixels as lesion pixels, over-estimating the lesion area.

Table 1: Segmentation results over all 200 images in $PH^2$ dataset.

| Method | Sensitivity | Specificity | Accuracy | F-score |
|---|---|---|---|---|
| JSEG[20] | 0.7108 | 0.9714 | $0.8947 \pm 0.0176$ | 0.7554 |
| SRM[21] | 0.1035 | 0.8757 | $0.6766 \pm 0.0346$ | 0.1218 |
| KPP | 0.4147 | 0.9581 | $0.7815 \pm 0.0356$ | 0.5457 |
| K-means | 0.7291 | 0.8430 | $0.8249 \pm 0.0107$ | 0.6677 |
| Otsu | 0.5221 | 0.7064 | $0.6518 \pm 0.0203$ | 0.4293 |
| Level Set[22] | 0.7188 | 0.8003 | $0.7842 \pm 0.0295$ | 0.6456 |
| ASLM[9] | 0.8024 | **0.9722** | $0.8966 \pm 0.0276$ | 0.8257 |
| Our method | **0.9104** | 0.8973 | $\mathbf{0.9039 \pm 0.1419}$ | **0.8918** |

We ran three different classification experiments to test the benefits of our proposed features. First, we experimented using a list of classic morphological features. In the second experiment, we used only the proposed shape and color features introduced in section 4. Finally, we ran an additional classification experiment using a combination of both sets of features.

Because the segmentation directly affects the region over which the features are computed; all the features were extracted over the segmented region that results from our superpixel segmentation with $k = 400$. As stated in subsection 3.1, this value of $k$ was selected because it yielded the best results in terms of segmentation.

The classic features were extracted from the segmented region using Scikit-Learn python library. Several image moments were included too along with classic color features over the whole segmented image. The set $F$ contains the asymmetry, border, and color features described in previous sections:

$$F = [F_{\text{asymmetry}}, F_{\text{border}}, F_{\text{color}}] \tag{5}$$

We used three classifiers for all the experiments: 1) logistic regression, 2) SVM, and 3) the fully connected neural network extracted from the VGG-16 deep learning architecture. For each algorithm, a 10-fold cross-validation was used with a partition of 90% for training and 10% for testing. We report mean accuracy, precision, recall, and F1-score over all the images in the dataset. Table 2 summarizes the results of our experiments in comparison with other studies in the state-of-the-art. All the metrics are the average values over the three classes of lesion, averaged over the ten folds of the cross-validation.

Note that when the classification uses only classical morphological features, the performance is significantly lower in comparison with the proposed features alone. We see this as an indication of the effectiveness our the proposed methodology to capture the morphological and color cues hold by the A, B, and C criteria in the ABCDE rule. Note that in most experiments, the higher performance in all metrics attained by combining classic and proposed features is small. Therefore, the contribution of classic features to the overall performance is marginal. While our classification strategy is not as accurate as the usage of deep neural networks, we achieved comparable results. Moreover, we did not simplify the problem by combining the two non-melanoma classes (common nevi and atypical nevi) into one.

The source code implementation of the presented study is publicly available*. The code for generating the segmentation was implemented in Python 2.7 while the feature extraction and classification steps were implemented in Python 3.6. Both implementations are based on the Scipy and Scikit libraries. All tests ran on a desktop machine with an Intel Core i7 processor of 2,5 GHz.

---

*https://github.com/dipaco/superpixel-skin-lesion-segmentation

| Feature set | Classifier | Accuracy | Precision | Recall | F1-Score |
|---|---|---|---|---|---|
| Logistic regression | Classic | 0.537 | 0.540 | 0.531 | 0.531 |
| | Proposed | 0.745 | 0.756 | 0.731 | 0.731 |
| | all | 0.761 | 0.770 | 0.751 | 0.755 |
| SVM | Classic | 0.545 | 0.555 | 0.522 | 0.522 |
| | Proposed | 0.625 | 0.630 | 0.620 | 0.620 |
| | All | 0.831 | 0.840 | 0.825 | 0.825 |
| Neural Network | Classic | 0.665 | 0.681 | 0.631 | 0.631 |
| | Proposed | 0.804 | 0.805 | 0.802 | 0.802 |
| | All | **0.865** | **0.870** | **0.855** | **0.855** |
| Deep CNN[23] | - | 0.875 | - | - | - |
| Bag of Words + SVM[24] * | - | **0.920**$^*$ | - | - | - |

Table 2: Classification results. Linear regression, support vector machines and a neural network were used to classify the skin lesions using three sets of features: Classic morphological and color features, our proposed features, and a combination of all features. Results shows how the inclusion of our proposed feature benefits the performance in all cases.

## 6. CONCLUSIONS AND FUTURE WORK

In this paper, we proposed a new set of shape-inspired feature for skin lesion classification, aiming to differentiate between three classes of lesion: 1) common nevus, 2) atypical nevus, and 3) melanoma. Our method uses the SLIC algorithm to over-segment the image, and then merge the resulting superpixels to produce two regions: healthy skin and skin lesion. Then a set of features based on the well-known ABCDE of melanoma are computed exploiting the properties of the contour such as symmetry and smoothness. For both segmentation and classification, our method gets close to the performance of deep learning algorithms on the small $PH^2$ dataset while requiring less computational resources.

Future work will focus on adjusting the merging criterion during segmentation to deal with cases where the lesion has more that one unconnected region. Regarding classification, a future work direction is to employ second-order textures to better represent the color structure of melanoma lesion in contrast to common and atypical nevus. Additionally, the use of methods to reduce class imbalance could also lead to significant improvement of the results.

## REFERENCES

[1] Tsao, H., Olazagasti, J. M., Cordoro, K. M., Brewer, J. D., Taylor, S. C., Bordeaux, J. S., Chren, M.-M., Sober, A. J., Tegeler, C., Bhushan, R., and Begolka, W. S., "Early detection of melanoma: Reviewing the abcdes," *Journal of the American Academy of Dermatology* **72**(4), 717 – 723 (2015). 1

[2] Ilyas, M., Costello, C. M., Zhang, N., and Sharma, A., "The role of the ugly duckling sign in patient education," *Journal of the American Academy of Dermatology* **77**(6), 1088 – 1095 (2017). 1

[3] Patino, D., Avendaño, J., and Branch, J. W., "Automatic skin lesion segmentation on dermoscopic images by the means of superpixel merging," in [*Medical Image Computing and Computer Assisted Intervention – MICCAI 2018*], Frangi, A. F., Schnabel, J. A., Davatzikos, C., Alberola-López, C., and Fichtinger, G., eds., 728–736, Springer International Publishing, Cham (2018). 1, 6

[4] Mendonc, T., Ferreira, P. M., and Marques, J. S., "PH 2 - A dermoscopic image database for research and benchmarking," in [*Annual International Conference of the IEEE Engineering in Medicine and Biology Society*], 5437–5440 (2013). 2, 5

[5] Celebi, M., Wen, Q., Iyatomi, H., Shimizu, K., Zhou, H., and Schaefer, G., "A state-of-the-art survey on lesion border detection in dermoscopy images," in [*Dermoscopy Image Analysis*], M. Emre Celebi, Teresa Mendonca, J. S. M., ed., 97–129, CRC Press (Sept. 2015). 2

[6] Celebi, M. E., Stoecker, W. V., and Schaefer, G., "Lesion Border Detection in Dermoscopy Images," *National Institute of Health Public Access* **33** (2010). 2

[7] Abuzaghleh, O., Barkana, B. D., and Faezipour, M., "Automated skin lesion analysis based on color and shape geometry feature set for melanoma early detection and prevention," in [*IEEE Long Island Systems, Applications and Technology (LISAT) Conference 2014*], 1–6, IEEE (may 2014). 2

[8] Barata, C., Celebi, M., and Marques, J., "Melanoma detection algorithm based on feature fusion," *Proceedings of the Annual International Conference of the IEEE Engineering in Medicine and Biology Society, EMBS* **2015-Novem**, 2653–2656 (2015). 2

[9] Pennisi, A., Bloisi, D. D., Nardi, D., Giampetruzzi, A. R., Mondino, C., and Facchiano, A., "Skin lesion image segmentation using Delaunay Triangulation for melanoma detection," *Computerized Medical Imaging and Graphics* **52**, 89–103 (2016). 2, 6, 7

[10] Sabbaghi, S., Aldeen, M., Garnavi, R., Varigos, G., Doliantis, C., and Nicolopoulos, J., "Automated colour identification in melanocytic lesions," in [*2015 37th Annual International Conference of the IEEE Engineering in Medicine and Biology Society (EMBC)*], 3021–3024, IEEE (aug 2015). 2

[11] Barata, C., Ruela, M., Francisco, M., Mendonça, T., and Marques, J. S., "Two systems for the detection of melanomas in dermoscopy images using texture and color features," *IEEE Systems Journal* **8**, 965–979 (Sep. 2014). 2

[12] Mahmoud, M. K. A., Al-Jumaily, A., and Takruri, M., "The automatic identification of melanoma by wavelet and curvelet analysis: Study based on neural network classification," in [*2011 11th International Conference on Hybrid Intelligent Systems (HIS)*], IEEE (Dec. 2011). 2

[13] Ballerini, L., Fisher, R. B., Aldridge, B., and Rees, J., "A color and texture based hierarchical k-NN approach to the classification of non-melanoma skin lesions," in [*Color Medical Image Analysis*], Schaefer, M. E. C., ed., 63–86, Springer Netherlands (2013). 2

[14] Kendall, D. G., "Shape manifolds, procrustean metrics, and complex projective spaces," *Bulletin of the London Mathematical Society* **16**(2), 81–121 (1984). 2

[15] Saha, P. K., Borgefors, G., and Sanniti di Baja, G., "A survey on skeletonization algorithms and their applications," *Pattern Recognition Letters* **76**, 3–12 (2016). 2

[16] Yang, M., Kpalma, K., and Ronsin, J., "A Survey of Shape Feature Extraction Techniques," in [*Pattern Recognition*], Yin, P.-Y., ed., 43–90, IN-TECH (Nov. 2008). 38 pages. 2

[17] Biasotti, S., Falcidieno, B., Giorgi, D., and Spagnuolo, M., [*Mathematical Tools for Shape Analysis and Description*], Synthesis Lectures on Computer Graphics and Animation, Morgan & Claypool Publishers (2014). 2

[18] Achanta, R., Shaji, A., Smith, K., Lucchi, A., Fua, P., and Süsstrunk, S., "SLIC superpixels compared to state-of-the-art superpixel methods," *IEEE Transactions on Pattern Analysis and Machine Intelligence* **34**, 2274–2282 (Nov. 2012). 3

[19] Dubuisson, M.-P. and Jain, A., "A modified Hausdorff distance for object matching," in [*Proceedings of 12th International Conference on Pattern Recognition*], **1**(1), 566–568, IEEE Comput. Soc. Press (2002). 5

[20] Zhao, Q., "JSEG method implementation," (2001). cs.joensuu.fi/zhao/Software/JSEG.zip. 7

[21] Boltz, S., "SRM method implementation," (2010). http://www.mathworks.com/matlabcentral/fileexchange/authors/73145. 7

[22] Crandall, R., "Level set implementation," (2000). https://github.com/rcrandall/ChanVese. 7

[23] Salido, J. A. A. and Conrado Ruiz, J., "Using Deep Learning for Melanoma Detection in Dermoscopy Images," *International Journal of Machine Learning and Computing* **8**(1), 61–68 (2018). 8

[24] Bi, L., Kim, J., Ahn, E., Feng, D., Fulham, M., Medicine, N., Prince, R., and Hospital, A., "Automatic Melanoma Detection via Multi-scale Lesion-biased Representation and Joint Reverse Classification," in [*2016 IEEE 13th International Symposium on Biomedical Imaging (ISBI)*], 1055–1058 (2016). 8